LANGMUIR

pubs.acs.org/Langmuir Article

Line Tension of Nanodroplets on a Concave Surface

Xiaojing Ma, Junpeng Lei, and Jinliang Xu*

Cite This: *Langmuir* 2021, 37, 4432−4440 Read Online

ACCESS | Metrics & More | Article Recommendations

ABSTRACT: The contact angle of a nanodroplet on a surface may deviate from that of a macrodroplet on a surface. Even though there are many studies regarding line tension, it is not well understood. In this paper, molecular dynamics simulation is performed for nanodroplets on a concave solid wall. The Lennard-Jones (L-J) potential is directly used or modified to simulate the force interaction between argon atoms and between solid−liquid particles. The initial droplet radius is 4, 5, and 6 nm, respectively. The k coefficient is defined as the ratio of the initial droplet radius with respect to the curvature radius of concave walls, which is in the range of 0−0.9, in which k = 0 refers to a flat surface. We found that indeed the contact angle θ of a nanodroplet on a concave wall deviates from that of a macrodroplet on a flat surface. Contact angles display a two region distribution, in which θ increases with increasing k for k < 0.5 and decreases with increasing k for k > 0.5. The k coefficient influences the droplet morphology. With k in the range of 0−0.9, the vapor−liquid interface is switched from a convex shape to a flat shape and finally reaches a concave shape. The line tension generally behaves in an increasing trend with the increase of k but becomes constant when k is beyond 0.7. The liquid densities, radial distribution functions, and coordination numbers show that the liquid particles are more closely packed with each other with the increase of k. The line tension achieves a positive sign and on the magnitude of 10^{-11} N, which has a linear increase with respect to the peak density of the first liquid layer.

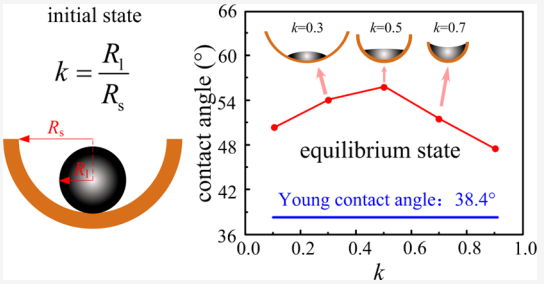

INTRODUCTION

Due to the fast development of micro-/nanofabrication techniques, solid structures can be fabricated in various shapes, including both the flat surface and concave surface.[1,2] The latter may be used for the dropwise condensation improvement. When the concave surface temperature is lower than the dew-point temperature, the vapor in the air can be nucleated to form many nanodroplets on the concave surface. When these droplets are mixed with each other, the coalescence-induced jumping takes place to enhance the dropwise condensation heat transfer.[3,4] This phenomenon can occur in nature as well as during the microfabrication process in a clean room.

The line tension can be neglected for macrosystems but is important for various applications in nanosystems. On the curved surface, on a nanoscale level, this force is of great significance for froth flotation, microporous solids, and condensation on nanorods.[5] Even though there are many studies available for line tensions in literature, there are no general conclusions that can be drawn till date. Dated back to 1878, Gibbs found that the interactions near the gas−liquid−solid three-phase contact line could not be treated by the free energies of each pair of phases alone.[6] Hence, he defined line tension as the excess energy per unit length of a contact line of three phases, analogous to surface tension, which is the excess free energy per unit area. Harkins estimated the magnitude of line tension based on energy conservation between free energy, latent heat of evaporation, and total energy.[7] Pethica defined the line tension on an ideal surface to give the modified Young equation as[8]

$$\cos\theta = \frac{\sigma_{sv} - \sigma_{sl}}{\sigma_{lv}} - \frac{\tau/\sigma_{lv}}{R_c} = \cos\theta_Y - \frac{\tau/\sigma_{lv}}{R_c} \quad (1)$$

where τ is the line tension, θ and θ_Y are the contact angle and the Young contact angle, respectively, and the subscripts s, l, and v represent the solid, liquid, and gas, respectively. R is the radius of curvature of a liquid droplet on an ideal solid surface at the equilibrium state with respect to the vapor phase. Dobbs and Indekeu studied the contact line between a thin film and a bulk liquid and calculated the line tension by employing an interface displacement model equivalent to Derjaguin's and de Gennes' approach.[9] Qu et al. proposed the gradient theory to calculate and analyze the line tension−free energy of a liquid−liquid−fluid three-phase contact line.[10] By considering the free energy to be dependent on the thickness and properties of the contact line, they used an extended gradient theory approach

Received: December 7, 2020
Revised: March 23, 2021
Published: April 6, 2021

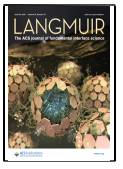

https://doi.org/10.1021/acs.langmuir.0c03489
Langmuir 2021, 37, 4432−4440

to evaluate the line tension of the contact zone. The theoretical outcomes with hexane−water−nitrogen and cyclohexane−water−nitrogen as working fluids agreed with the existing experimental data.

The line tension is influenced by various factors, including the ratio of the droplet size and the radius of surface curvature, characteristic angle, wall roughness, and so forth . Schimmele et al.[11,12] studied liquid−liquid−gas and gas−liquid−solid systems. They defined line tensions in two different ways, showing identical contact angles based on different definitions of line tensions. Guzzardi and Rosso[13] studied the effect of the radius of curvature on droplet wettability and analyzed the sign of line tensions. They showed that compared to the positive line tension, with the negative line tension, it is easier to make the droplet stabilize on the curved surface. Hienola et al.[14] evaluated the contact angle and the line tension based on heterogeneous bubble nucleation data, showing larger microscopic contact angles than those in the macroscale. The line tension got a negative value and decreased the energy barrier for bubble nucleation and thereby shortened the bubble nucleation time. Checco and Guenoun[15] measured the contact angle of microsized and nanosized alkane droplets partially wetting a model substrate using noncontact atomic force microscopy. The contact line curvature was determined dependent on the contact angle with unprecedented accuracy. The line tension is measured to be negative and on the magnitude of 10^{-10} N. Gu et al.[16,17] studied the size effect of the contact angle in the solid−oil−water system and explored its relationship with respect to line tension. Positive line tension was detected and about 8.2×10^{-7} N. The line tension effect becomes more obvious with a decrease of droplet volumes. On the other hand, Leelamanie and Karube[18] identified a positive line tension which is on the order of 10^{-5} N.

In summary, both theoretical and experimental works have been done on line tensions. The measured line tensions are in a very wide range of 10^{-12} to 10^{-5} N with an uncertain sign. Based on microscopic density functional theory, Bauer and Dietrich[19] calculated the internal structure of the three-phase contact line and the morphology of liquid wetting films on a substrate. The numerical simulations are compared with those predicted by a simple phenomenological interface displacement model. They found that the interface displacement model provides a quantitatively reliable description of the interfacial structures. Churaev et al.[20] derived an analytical expression for line tension for the disjoining pressure isotherm in a simplified form. The line tension is shown to depend not only on the isotherm parameters but also on the radius of the three-phase contact perimeter. Park et al.[21] used molecular dynamics to investigate the wetting characteristics such as contact angle, wetting radius, and topography of water droplets on smooth and random solid surfaces. For weak interaction between the solid and liquid, the contact angle is less affected by surface roughness. However, for strong interaction between the solid and liquid, contact angles are influenced by both the droplet size and surface roughness. Weijs et al.[22] computed the shape of Lennard-Jones nanodrops using molecular dynamics and compared them to density functional theory. The deviation from Young's law was very small and would correspond to a typical line tension length scale (defined as line tension divided by surface tension) similar to the molecular size and decreasing with Young's angle. Peng et al.[23,24] numerically simulated cylindrical and spherical nanodroplets for comparison. The contact angles from the cylindrical drops and Young's equation agree very well over the range of surface strengths and cylindrical drop sizes, except on a very weak surface. For spherical droplets, a deviation between the contact angle of spherical droplets and Young's equation was evident but decreased with increasing interaction strengths to be negligible for contact angles less than 90°.

The above literature survey indicates that most of the nanodroplet wetting studies were investigated on flat surface. The studies on the curved surface are not sufficient. In this paper, we investigate the nanodroplet wetting on concave surface, focusing on the effects of the droplet size and curvature radius of the solid wall. The behavior is finally correlated with the fluid density amplitude of the first fluid layer.

NUMERICAL METHOD

Figure 1a shows the simulation box to study the nanodroplet wetting on the concave surface. The box had a size of 34.05 nm

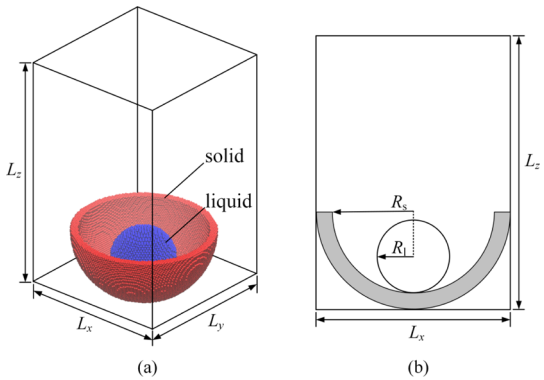

Figure 1. Physical problem studied in this study (a: 3D configuration; b: 2D configuration).

× 34.05 nm × 51.08 nm for L_x, L_y, and L_z, respectively. Periodic boundary conditions are applied along x and y directions. The solid wall consists of five layers of atoms, arranged in the face-centered-cubic (fcc) form with a lattice constant of 1.5σ and with the ⟨111⟩ crystal plane directly contacting liquid argon. Figure 1b shows the physical problem over the xz plane, symmetrized against the half plane in the y direction, where R_l is the droplet radius and R_s is the radius of the curvature of the solid wall. In our study, different R_s are used, corresponding to the number of solid wall atoms in the range of 8555−56,081. Based on previous studies, only very tiny droplets can have line tension.[9,11,12] Hence, three droplet radii are selected as R_l = 4, 5, and 6 nm, corresponding to the number of liquid atoms of 5298, 10,305, and 17,856, respectively. It is noted that surface tension between the solid and liquid (σ_{lv}) is dependent on the droplet size in nanoscale. However, previous studies show that σ_{lv} is changed by 5% corresponding to the 7 nm variation of droplet radii.[25] Hence, it is reasonable to assume the constant surface tension in a narrow range of R_l = 4, 5, and 6 nm in this paper.

During simulation, the solid atoms are stationary. Initially, liquid atoms are also arranged according to the fcc structure but will be moving once the simulation is initiated. The argon liquid is used, with a lattice constant of 1.72σ. Initially, liquid density is set as $\rho\sigma^3 = 0.78$, where ρ is the number of particles per unit volume, and σ is the length scale of the liquid atom.

https://doi.org/10.1021/acs.langmuir.0c03489
Langmuir 2021, 37, 4432−4440

An important parameter k is defined as the ratio of the droplet radius relative to the radius of curvature of the solid wall, $k = R_l/R_s$. Examining eq 1 identifies that once the characteristic contact angle θ_Y for a macrodroplet on a flat surface is fixed, the cosine component of θ_Y has the same effect on θ for different k. The Newton equation is written for each liquid atom as

$$m\frac{d\vec{r}^2}{dt^2} = \sum_{j\neq i,j=1}^{N} \vec{F}_{ij} + \sum_{j_s\neq i,j=1}^{N_s} \vec{F}_{ij_s} \quad (2)$$

where F_{ij} refers to the pair interaction force between liquid atoms, and F_{ij_s} represents the pair interaction force between the liquid and solid atoms, r is the distance between two atoms, and N and N_s are the number of liquid atoms and solid atoms, respectively. The pair interaction force is

$$F_{ij} = -\frac{\partial \phi_{ij}}{\partial r_{ij}} \quad (3)$$

The potential for liquid−liquid interaction is written as

$$\phi(r) = 4\varepsilon\left[\left(\frac{\sigma}{r}\right)^{12} - \left(\frac{\sigma}{r}\right)^{6}\right] \quad (4)$$

where σ is the length scale of the argon atom ($\sigma = 0.3405$ nm), ε is the energy scale of the argon atom $\varepsilon = 1.67 \times 10^{-21}$ J), and m is the mass of an argon atom ($m = 6.69 \times 10^{-23}$ g). We also use eq 4 for the pair interaction between solid atoms, using $\sigma_s = 0.2475$ nm and $\varepsilon_s = 8.35 \times 10^{-20}$ J to replace σ and ε, respectively. The potential between the solid−liquid interaction is given as follows[26]

$$\phi(r) = 4\alpha\varepsilon_{sl}\left[\left(\frac{\sigma_{sl}}{r}\right)^{12} - \beta\left(\frac{\sigma_{sl}}{r}\right)^{6}\right] \quad (5)$$

where ε_{sl} and σ_{sl} are the energy scale and the length scale for solid−liquid interactions, respectively, which are decided by the Lorentz−Berthelot principle,[27] $\varepsilon_{sl} = \sqrt{\varepsilon_l \cdot \varepsilon_s}$ and $\sigma_{sl} = (\sigma_s + \sigma_l)/2$. The subscripts s and l represent the solid and the liquid, respectively. The parameters α and β are used to adjust the intensity of the interaction between the solid and the liquid. In this paper, $\alpha = 0.14$ and $\beta = 0.7$ are used, corresponding to a contact angle of 38.4° hydrophilic wettability for a macroscale droplet on an ideal flat surface.[27]

The Velocity-Verlet algorithm method is used to solve eq 1. The timestep is set as $\Delta t = 4.66 \times 10^{-4}\ \tau$, corresponding to 1 fs, where τ is the timescale for argon, $\tau = \sqrt{m\sigma^2/\varepsilon}$. The simulation system is kept at a constant temperature of $T = 0.827\ \varepsilon/k_B$, where k_B is the Boltzmann constant. Totally, each case runs four million steps, among which the first two million steps are used for the system to reach the equilibrium state, and the latter two million steps are used for the statistical analysis of the computed data.

Figure 2 shows two independent systems to obtain the surface tension of γ_{lv} between the vapor and liquid. A system size of 6.81 nm × 6.81 nm × 17.03 nm is shown in Figure 2a. The surface area between the liquid and vapor is recorded as A. Initially, the bottom part of the box contains liquid atoms based on the fcc structure. The system energy is recorded as E_{uni} after the equilibrium state is reached. An alternative way is to arrange the whole liquid atoms into two equal parts (see Figure 2b). Hence, the surface area between the vapor and liquid is 2A. The finally obtained system energy is recorded as E_{sep}. The surface tension γ_{lv} is written as

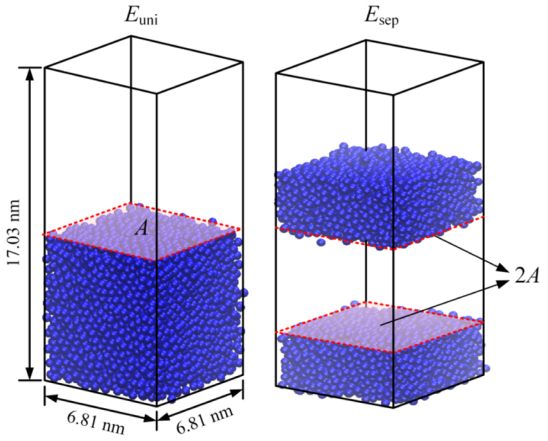

Figure 2. Physical system to determine the surface tension between the vapor and the liquid (a: one surface between the vapor and the liquid; b: two surfaces between the vapor and the liquid).

$$\gamma_{lv} = \frac{E_{sep} - E_{uni}}{2A} - T\frac{S_{sep} - S_{uni}}{2A} \approx \frac{E_{sep} - E_{uni}}{2A} \quad (6)$$

The second term of the right side of eq 6 is contributed by entropy increase, which can be neglected compared to the first term of the right side of eq 6, where S is the entropy and T is the temperature. The system is simulated under the NVT condition with the total number of argon atoms of 6000. The system temperature is well controlled to be $T = 0.827\ \varepsilon/k_B$. Finally, the value of $\gamma_{lv} = 9.0452 \times 10^{-3}$ N/m is obtained, matching the value reported in the literature.[28]

Due to the simple structure of argon with one atom only, the MD simulation saves computation resource. Because the contact angle on the concave surface is dependent on the Young contact angle θ_Y and the k value, the results in this paper can be extended to other complex fluids such as water. In this relationship, θ_Y is dependent on the molecular interaction between the solid and liquid, and k is the size parameter. Thus, if the pair interaction intensity between a complex fluid and solid is the same as that between argon and the solid, the contact angles are almost the same for the two systems.

RESULTS AND DISCUSSION

Nanodroplet Wettability on the Concave Surface. Figure 3 shows the nanodroplet wetting on concave surface with $k = 0.1$, 0.3, 0.5, 0.8 and 1.0, respectively. The droplet radius is $R_l = 5$ nm. At the initial state, the droplet just contacts the bottom of the concave surface. With time evolving and due to the attraction of the solid−liquid interaction, the droplet is elongated in the z direction to form an oval droplet in the top. The liquid atoms are adhered on the wall at the bottom part, and the three-phase contact line is spreading along the concave surface. The top droplet surface gradually becomes flatter, leaving residual atoms distributed elsewhere as the vapor in the box. Once the equilibrium state is reached, the contact angle obviously appears. Due to the confinement by the concave wall and the attraction between the solid and liquid, the top part of the droplet is gradually switched from the convex shape to a flat shape and finally reaches the concave shape, with an increase of k from 0.1 to 0.9.

https://doi.org/10.1021/acs.langmuir.0c03489
Langmuir 2021, 37, 4432−4440

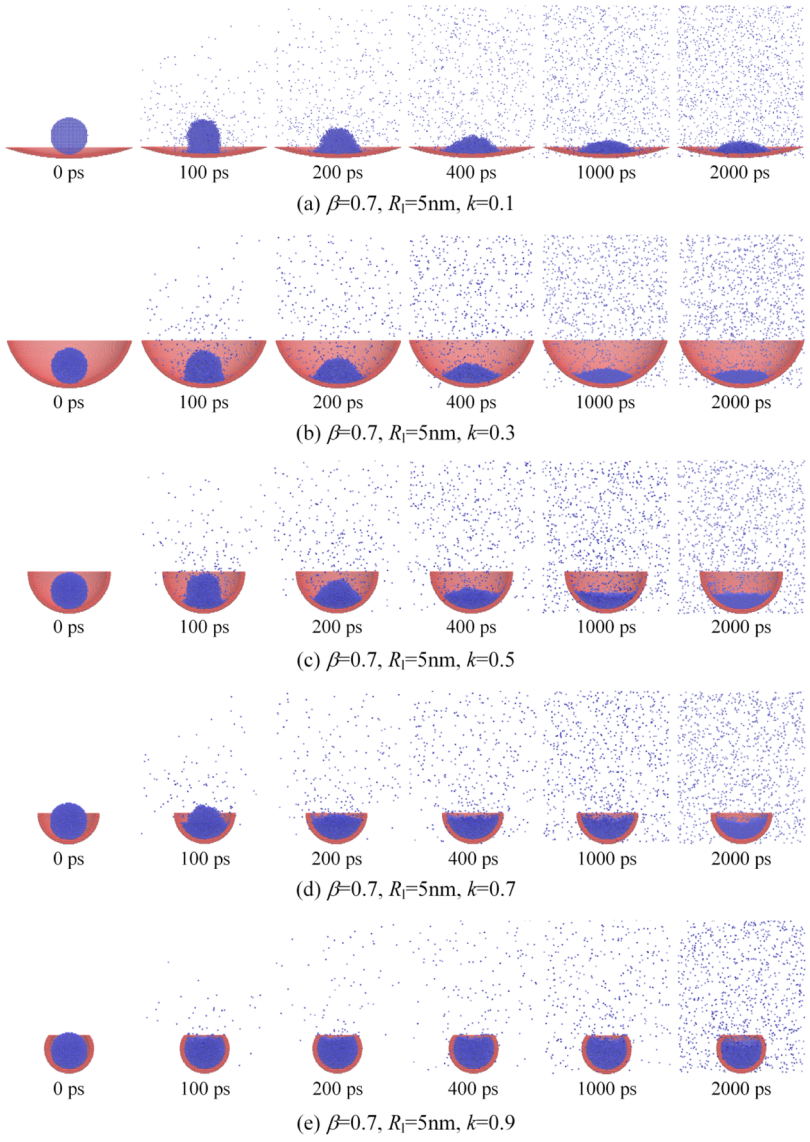

Figure 3. Wetting process for a nanodroplet on a concave wall at different k.

Here, the contact angle is obtained via a method of the identical fluid density profile by establishing a cylindrical coordinate characterized by a radial coordinate r and a height coordinate z (see Figure 4a). The system is subdivided into 750 × 250 grids, each grid having $\Delta r = \Delta z = 0.2\sigma$. Figure 4b shows the droplet morphology and the definition of the contact angle. After the equilibrium state is reached, the fluid density distribution over the xz plane is deduced. An important task is to achieve the vapor−liquid interface location and the vapor−liquid−solid contact point. As shown in Figure 4b, the solid substrate height is s and the liquid height is h. The vapor−liquid interface is defined at the location where the density is $\rho^* = 0.5(\rho_l + \rho_v)$, where ρ_l and ρ_v are the liquid density in the bulk liquid region and vapor density in the bulk vapor region, respectively. The contact angle is the angle between two tangent lines of the vapor−liquid interface and the solid wall at the three-phase contact point. Figure 4c shows the density profile in the fluid region excluding the solid wall, showing the oscillating $\rho\sigma^3$ within the liquid region but a flat distribution in the vapor region. Hong et al.[28] gives the theoretical density distribution at z as follows

$$\rho(z) = \frac{1}{2}(\rho_l + \rho_v) - \frac{1}{2}(\rho_l - \rho_v) \times \tan h\frac{2(z - z_0)}{d} \quad (7)$$

where d is the thickness of the vapor−liquid interface and z_0 is the center location of the vapor−liquid interface. Figure 4c shows the agreement between the average densities determined by MD simulations and the theoretical determined values.

One may be interested in the evolution of the droplet morphology and contact angles on a concave surface (see Figure 5 with R_l = 5 nm and k = 0.5). At the initial time t = 0, a droplet with its radius of 5 nm is standing on the bottom of a concave bowl. The contact angle is 180° at t = 0. Based on the arrangement of liquid atoms at t = 0, the thickness of the vapor−liquid interface is zero also called the mathematical thickness. With time evolving, the thickness of the vapor−liquid interface is not zero anymore but reaches a limited value within ∼1σ, where σ is the characteristic length of a single argon atom. Across the two sides of the interface thickness is the bulk liquid with densely populated atoms and the bulk vapor with sparsely populated atoms. The contact point is the

https://doi.org/10.1021/acs.langmuir.0c03489
Langmuir 2021, 37, 4432−4440

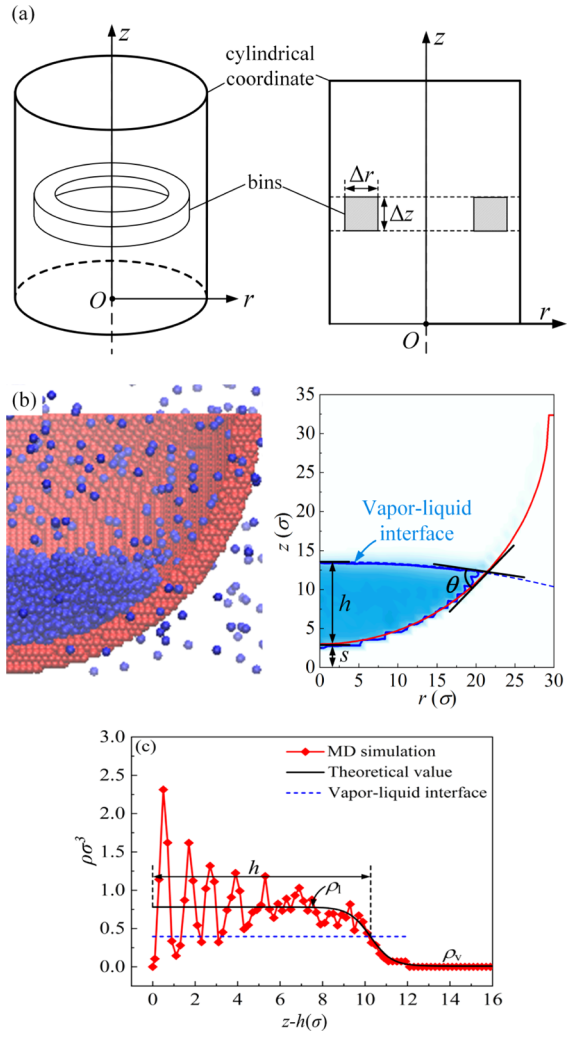

Figure 4. Cylindrical coordinate system to determine the fluid density distribution (a: cylindrical coordinate; b: 2D density distribution; c: fluid density vs distance away from the solid wall).

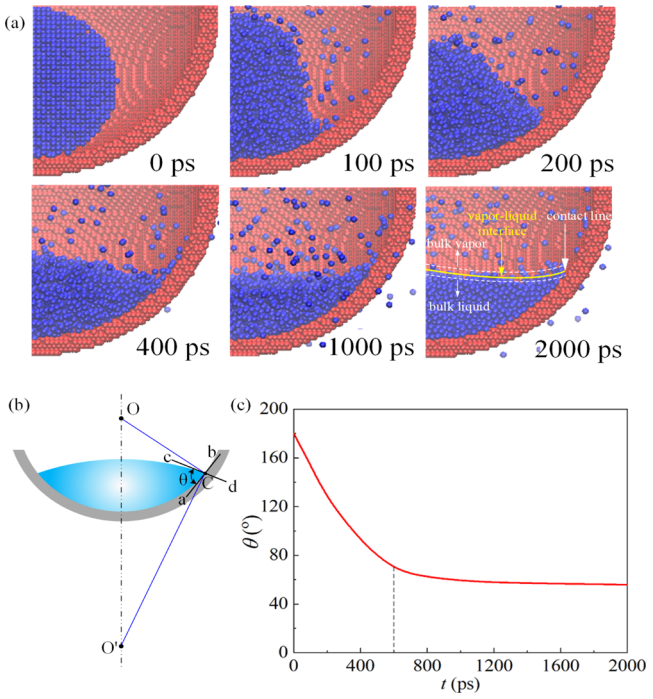

Figure 5. Dynamic droplet morphology and contact angles for 5 nm droplet on the concave surface (a: droplet morphology; b: geometric parameters defining the contact angle; c: contact angles vs time).

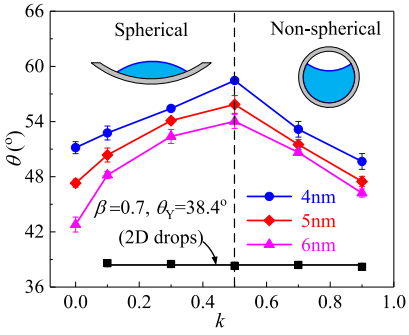

Figure 6. Contact angles versus k at different droplet sizes.

point at which the gas−liquid interface intercrosses with the concave surface, while the contact line is the collection of contact points along the circumference direction on the concave surface. Droplet patterns are shown at t = 0, 100, 200, 400, 1000, and 2000 ps (see Figure 5a). Having the droplet morphology and the definition of the vapor−liquid interface and contact line, one can have the geometry picture showing both the droplet and concave wall (see Figure 5b). The contact angle for the nanodroplet on the concave surface is the angle between the two tangent lines of *ab* and *cd*. Figure 5c shows dynamic contact angles θ versus time. It is seen that θ quickly decreases from 180° at t = 0 within an initial transition stage of ∼600 ps. Beyond the transition stage, θ slowly decreases and finally stabilizes at 55.7°, which is called the equilibrium contact angle.

Contact angle θ versus k is shown in Figure 6, in which R_l = 4, 5, and 6 nm are presented. Two types of droplet morphologies appear on the concave solid wall, symmetrically distributed against at k = 0.5. The droplet displays a convex shape with k < 0.5 but a concave shape with k > 0.5. The θ increases with increasing k with k < 0.5 but decreases with increasing k with k > 0.5. This variation trend is the same for any droplet size, attaining the maximum contact angle at k = 0.5. Figure 6 emphasizes the important effect of the curvature of the concave wall on contact angles. We remember that k = 0 belongs to the flat surface. For example, when the line tension effect is considered with the droplet size of 4 nm, the contact angle is θ = 51.2° on a flat surface (k = 0) but is increased to 58.4° on a concave surface (k = 0.5). The increased trend of contact angles is also observed from k = 0 to 0.5 with droplet sizes of 5 and 6 nm (see Figure 6).

We note that the present work focusses on 3D simulation results. To explore the effect of 2D and 3D on nanodroplet wetting, additional 2D simulations are performed, containing a concave cylinder shell for the solid and 2D droplet for the liquid. The contact angle keeps a constant value of 38.4° at β = 0.7 with different k. The θ = 38.4° is exactly equal to that on the flat surface. The 2D droplet wettability is not influenced by the solid wall curvature, matching the results reported in the literature.[22−24] The line tension effect does not occur for the 2D droplet but becomes important for the 3D droplet, showing the strong 3D effect. Wolansky and Marmur[29] demonstrated that the droplet contact angle is not influenced by the solid wall curvature without considering line tension. The effect of

https://doi.org/10.1021/acs.langmuir.0c03489
Langmuir 2021, 37, 4432−4440

droplet size on wettability is also identified in Figure 6, showing that larger 3D droplet wettability gradually approaches that on the flat wall.

Figure 6 presents a clue to judge the criterion under which the line tension effect is important. Two parameters influence the contact angle on the concave surface (θ): the characteristic contact angle for macrodroplets on the flat surface (θ_Y) and the k value. We note that the k = 0 case belongs to the flat surface. For very small droplets such as 4, 5, and 6 nm, the line tension effect cannot be neglected even on a flat surface. This is because θ and θ_Y show apparent difference for these small droplets. One may be interested to know the critical droplet size beyond which the line tension effect disappears. Because k = 0.5 demonstrates the largest line tension effect, examining that the data trend at k = 0.5 estimates the critical droplet size. With the droplet sizes from 4 to 6 nm, the contact angle gradient is (1.8−2.7)°/nm. Assuming the average value of 2.2°/nm, the droplet radius of 13 nm will yield the same contact angle θ as θ_Y by such data extension. In one word, the droplet size beyond 13 nm does not have the line tension effect. This is why many authors investigate the line tension effect with droplet sizes smaller than 10 nm.[22,24,28]

Figure 7 shows contact radius R_c and droplet radius R_d versus k, displaying the two region distribution interfaced at k = 0.5. For k < 0.5, the convex vapor−liquid interface yields nearly constant contact radii R_c at different k. For k > 0.5, R_c sharply decreases, which is due to the decreased internal volume enclosed by the concave solid wall to elevate the contact line position. R_d also has two region distribution. R_d increases with increasing k for k < 0.5, corresponding to the convex vapor−liquid interface of a droplet on the concave solid wall. The vapor−liquid interface nearly becomes flat at k = 0.5, beyond which the vapor−liquid interface becomes concave to decrease R_d.

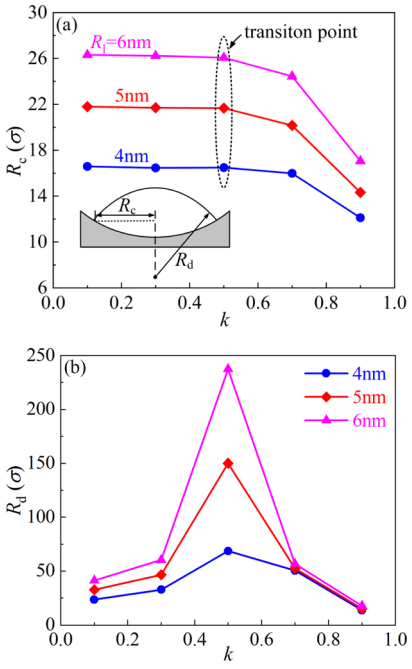

Figure 7. Contact radii of the solid−liquid−vapor three-phase contact line R_c (a) and the radii of the solid wall curvature R_d (b) versus k at different droplet sizes.

Line Tension of the Nanodroplet on the Concave Surface. To calculate the line tension of the nanodroplet on the concave surface, it is necessary to consider the curvature of the solid wall and droplet morphology. Equation 1 is revisited to deal with the two types of droplet morphologies at the equilibrium state (see Figure 8). Due to the curvature of the solid wall, the line tension component is not parallel to the surface tension of σ_{sl} between the solid and liquid. Hence, eq 1 cannot be used to compute the line tension directly. To overcome this issue, Hienola et al.[9] obtained the following equation

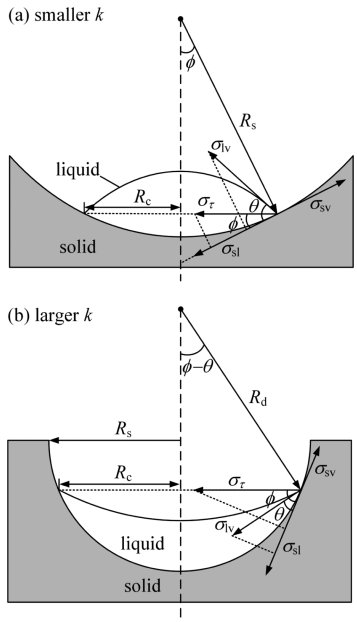

Figure 8. Force analysis of the nanodroplet on the concave surface.

$$\sigma_{sv} - \sigma_{sl} - \sigma_{lv}\cos\theta - \sigma_\tau\cos\phi = 0 \quad (8)$$

where θ is the contact angle, ϕ is the angle between the plane of the vapor−liquid−solid three-phase contact line and the solid−liquid interface, and σ_τ is the line tension component, pointing the circle center of the contact line

$$\sigma_\tau = \tau/R_c \quad (9)$$

where τ is the line tension. Combining eqs 8 and 9 and referring to Figure 8 yield

$$\sigma_{sv} - \sigma_{sl} - \sigma_{lv}\cos\theta - \frac{\tau}{R_s\tan\phi} = 0 \quad (10)$$

Rewriting eq 10 yields the relationship between cos θ and R_s and τ

$$\cos\theta = \cos\theta_Y - \frac{\tau}{\sigma_{lv}}\frac{1}{R_s\tan\phi} \quad (11)$$

$$\tau = \sigma_{lv}(\cos\theta_Y - \cos\theta)/\left(\frac{1}{R_s\tan\phi}\right) \quad (12)$$

Figure 9a plots the linear relationship between cosθ and $1/(R_s\tan\phi)$, in which simulation data points are shown and the linear curves are based on the correlation of the simulation results, covering the range of k from 0.1 to 0.9. It is emphasized that our work is performed at α = 0.14 and β = 0.7, under

https://doi.org/10.1021/acs.langmuir.0c03489
Langmuir 2021, 37, 4432−4440

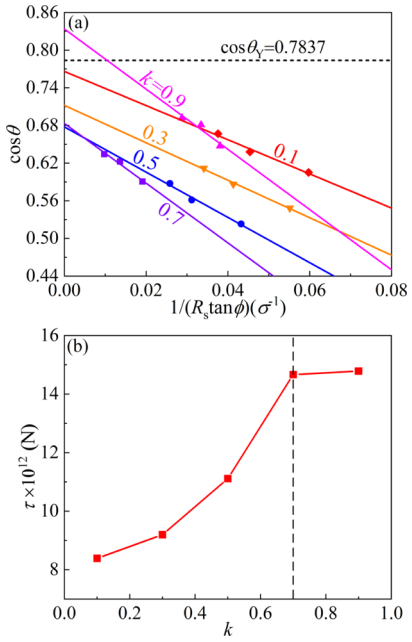

Figure 9. Variation trend of cos θ and line tension.

which the Yong contact angle is θ_Y = 38.4° corresponding to cos θ_Y = 0.7837.[21] Figure 9a tells us that contact angles in nanoscale, θ, indeed deviate from that on the macroscale, and they are influenced by both k and R_s (curvature radius of the solid wall). We note that the gradient of the line is the characteristic length of line tension, $l = -\tau/\sigma_{lv}$. The nonparallel lines at different k indicate that the characteristic lengths of line tension are different at different k. The line tension is actually the slope of the line timing the surface tension of σ_{lv} between the vapor and liquid. The negative slopes of the lines correspond to positive line tension, which are different at different k.

Because surface tension between the vapor and liquid is not changed, the line tension is linearly proportional to the characteristic length of line tension l. Based on Figure 9a, we achieve the line tension shown in Figure 9b. It is seen that the line tension is positive and on the magnitude of 10^{-11} N. When k is smaller than 0.7, the line tension is increased with an increase of k due to the effect of the curvature of solid wall. Beyond the k value of 0.7, the line tension almost does not change.

As mentioned in Introduction, line tension can be either negative[14,15] or positive.[16−18] The present paper identifies positive line tension. The sign of line tension is dependent on surface wettability, characterized by the contact angle θ_Y for a macrodroplet on a flat surface. For hydrophilic wall with θ_Y = 38.4° such as encountered in this paper, line tension is positive. Otherwise, line tension is negative for nanodroplets on a hydrophobic wall.

Factors Dominating Line Tension. To explain the mechanism that governs the variation of line tension, two parameters are introduced. The first one is the radial distribution function, RDF, recorded as $g(r_c)$, characterizing the local density fluctuation with a distance r_c from the center of a specific atom or molecule.

$$g(r_c) = \frac{1}{\rho_{ave} 4\pi r_c^2 \delta r_c} \frac{\sum_{t=1}^{N_t} \sum_{j=1}^{N} \Delta N(r_c \to r_c + \delta r_c)}{N \times N_t} \quad (13)$$

where N_t is the total steps for the integration and ΔN is the number of particles for a size interval from r_c to $r_c + \delta r_c$. The $g(r_c)$ approaches 1 when $r_c \to \infty$.

The second one is the coordination number, coord, which is the number of atoms or molecules in a r_x radius sphere, describing the microscopic structure of matter.

$$\text{coord} = \int_0^{r_x} g(r_c) 4\pi \rho_{bulk} r_c^2 dr_c \quad (14)$$

where ρ_{bulk} is the bulk number density. The large the coord is, the closer arrangement of atoms or molecules is.

Figure 10a shows the oscillating $\rho\sigma^3$ versus $z - h$, distance away from wall. The oscillating amplitudes are decayed with

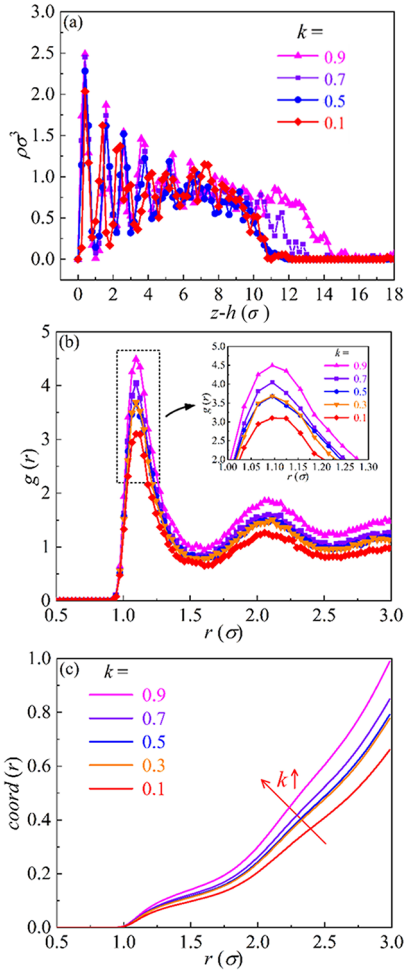

Figure 10. Fluid density versus distance away from the wall (a), radial distribution function $g(r_c)$ (b), and coordination number (c).

the increase of this distance. The first peak values of $\rho\sigma^3$ attain 2.03, 2.28, and 2.49 at k = 0.1, 0.5, and 0.9, respectively. The location for the first peak occurring almost does not change at different k. We conclude that the line tension is strongly related to the density of liquid particles near the wall (see Figures 9b and 10a). Similar variation trend of the radial distribution function, $g(r_c)$, is identified at different k (see Figure 10b). However, the peak values are increased with an increase of k, indicating more closely arranged liquid atoms at larger k, due to the enhanced confinement of the liquid in the internal volume with a concave wall. Alternatively, Figure 10c

https://doi.org/10.1021/acs.langmuir.0c03489
Langmuir 2021, 37, 4432−4440

shows the monotonic increase of the coordination number with the increase of k.

Finally, we present the linear relationship between line tension and the peak density of the first liquid layer (see Figure 11). The logic of the effect of k on line tension is explained as

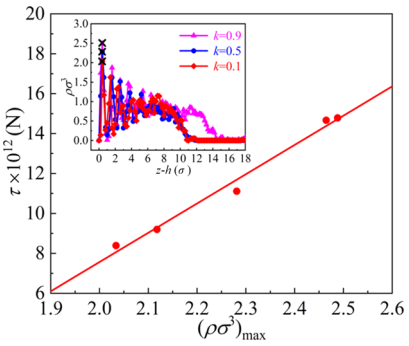

Figure 11. Linear relationship between the line tension and the peak density of the first liquid layer.

follows. A specific combination of droplet radius R_l (initial state) and curvature radius of concave wall R_s forms a coefficient k. The solid−liquid interaction is enhanced when k increases due to the confinement of the concave wall. This effect ensures more atoms or molecules attracted by the solid wall to increase the line tension. The major finding is that the line tension is linearly proportional to the peak density of the first liquid layer.

k = 0.7 is identified as the transition point for line tension (see Figure 9). The k is the initial droplet radius (R_l) divided by the curvature radius of the concave wall (R_s, see Figure 1). For a fixed R_l such as 5 nm presented in Figures 9−11, a smaller k corresponds to a larger bowl with a smaller height. A larger k corresponds to a smaller bowl with a larger height. By increasing k, the interaction between the droplet and concave wall becomes enhanced due to a larger contact area between the liquid and solid, explaining the increased line tension with increase of k. The solid−liquid interaction becomes sufficient for k > 0.7, yielding the constant density peak of the first liquid layer with k = 0.7 and 0.9 (see Figure 10a). Because line tension is linearly proportional to the density peak of the first liquid layer (see Figure 11), the line tension is not changed beyond k = 0.7 (see Figure 9).

We note that positive line tension is concerned due to hydrophilic wettability (θ_Y = 38.4°). This wettability enhances molecular interaction between the solid−liquid. Thus, liquid density displays a peak phenomenon near the wall. A hydrophobic wall may yield negative line tension, under which the density peak of the first liquid layer decreases, due to weak interaction between the solid and liquid.

In summary, we identify the important line tension effect for small droplets in nanoscale. The line tension effect cannot be neglected even on the flat surface. The concave surface enhances the line tension effect. For example, considering the Young contact angle of 38.4° in this paper, a 4 nm droplet has a contact angle of 51.2° on the flat surface but increases the contact angle to 58.4° on the concave surface at k = 0.5 (see Figure 6). This indicates the droplet size effect, which attains a ∼13° difference of contact angles between a macrodroplet (Young contact angle) and a 4 nm droplet. Also, this indicates an apparent curvature radius effect of concave wall, which attains a ∼7° difference of contact angles between the flat surface with k = 0 and concave surface with k = 0.5.

By extending the data trend obtained in this paper, we claim a critical droplet radius of ∼13 nm, before which the line tension effect cannot be neglected but beyond which the line tension effect is insignificant. Hence, the droplet size is a key parameter to determine if the line tension effect should be considered. Due to difficulties in measuring the droplet morphology for very small droplets, experimental evidence for line tension effect cannot be presented yet, but will be done in the future, if the measurement resolution is improved. This is the reason why many authors investigated the line tension effect using small droplets in ∼10 nm scale[22,24,28] and almost all of the studies in this area focus on the MD simulations. However, experimental evidence is presented in the literature for larger droplets in micron or millimeter scale, under which contact angles are the same on the flat surface, concave surface, and convex surface.[30,31]

CONCLUSIONS

When the droplet size is decreased to a nanoscale, the contact angle concept that is widely applied in the macroscale is not valid to describe the wetting process of the droplet on solid walls. In the present work, we focus on the numerical simulation and analysis of the nanodroplet on concave solid walls, using the molecular dynamics simulations. The Lennard-Jones (L-J) potential is used to simulate the force interaction between argon atoms, and it is modified to simulate the solid−liquid interaction by introducing two strength coefficients α and β. The selected values of α and β ensure a 38.4° contact angle of a macrodroplet on a flat surface. The initial droplet radius is 4, 5, and 6 nm. The k coefficient is in the range of 0.1−0.9. Following conclusions can be drawn:

1. Contact angles θ of nanodroplets on concave solid walls deviate from that of macrodroplets on a flat surface. For example, θ is 58.5° for a 4 nm radius droplet with k = 0.5, which is different from the Young contact angle of 38.4°. Contact angles display the two region distribution, in which θ increases with increasing k for k < 0.5 and decreases with increasing k for k > 0.5.
2. The initial droplet size and the curvature radius of the concave wall influence the droplet morphology. With k in the range of 0.1−0.9, the vapor−liquid interface is switched from a convex shape to a flat shape and finally reaches the concave shape. Both the contact radius of the three-phase contact line R_c and the droplet radius at the equilibrium state R_d display the two region distribution, interfaced at k = 0.5.
3. In the present work, the line tension generally behaves with the increasing trend with the increase of k but becomes constant when k is beyond 0.7. The liquid densities, radial distribution functions $g(r_c)$, and coordination number show that the liquid particles are more closely packed with each other with the increase of k. The line tension achieves a positive sign with the magnitude of 10^{-11} N, which has a linear relationship with respect to the peak density of the first liquid layer.

AUTHOR INFORMATION

Corresponding Author

Jinliang Xu − *Beijing Key Laboratory of Multiphase Flow and Heat Transfer for Low Grade Energy Utilization and Key*

https://doi.org/10.1021/acs.langmuir.0c03489
Langmuir 2021, 37, 4432−4440

Laboratory of Power Station Energy Transfer Conversion and System of Ministry of Education, North China Electric Power University, Beijing 102206, P.R. China; orcid.org/0000-0003-0145-9983; Email: xjl@ncepu.edu.cn

Authors

Xiaojing Ma − *Beijing Key Laboratory of Multiphase Flow and Heat Transfer for Low Grade Energy Utilization and Key Laboratory of Power Station Energy Transfer Conversion and System of Ministry of Education, North China Electric Power University, Beijing 102206, P.R. China*

Junpeng Lei − *Rundian Energy Science and Technology Co., Ltd, Zhengzhou 450046, P.R. China*

Complete contact information is available at: https://pubs.acs.org/10.1021/acs.langmuir.0c03489

Notes

The authors declare no competing financial interest.

■ ACKNOWLEDGMENTS

The authors acknowledge the support from the Nature Science Foundation of China (51821004).

■ REFERENCES

(1) Dawande, S. Heat transfer: Annular flow at concave surfaces. *Chem. Eng. World* **2004**, *39*, 78−80.
(2) Grabarnik, S.; Emadi, A.; Wu, H.; de Graaf, G.; Wolffenbuttel, R. F. Microspectrometer with a concave grating fabricated in a MEMS technology. *Procedia Chem.* **2009**, *1*, 401−404.
(3) Liu, T. Q.; Sun, W.; Sun, X. Y.; Ai, H. R. Mechanism study of condensed drops jumping on super-hydrophobic surfaces. *Colloids Surf., A* **2012**, *414*, 366−374.
(4) Xie, J.; Xu, J.; Shang, W.; Zhang, K. Dropwise condensation on superhydrophobic nanostructure surface, part II: Mathematical model. *Int. J. Heat Mass Transfer* **2018**, *127*, 1170−1187.
(5) Amirfazli, A.; Neumann, A. W. Status of the three-phase line tension: a review. *Adv. Colloid Interface Sci.* **2004**, *110*, 121−141.
(6) Gibbs, J. W. The Collected Works of J. Willard Gibbs. *Nature* **1929**, *124*, 119−120.
(7) Harkins, W. D.; William, D. Linear or Edge Energy and Tension as Related to the Energy of Surface Formation and of Vaporization. *J. Chem. Phys.* **1937**, *5*, 135−140.
(8) Pethica, B. A. The contact angle equilibrium. *J. Colloid Interface Sci.* **1977**, *62*, 567−569.
(9) Dobbs, H. T.; Indekeu, J. O. Line tension at wetting: interface displacement model beyond the gradient-squared approximation. *Phys. Stat. Mech. Appl.* **1993**, *201*, 457−481.
(10) Qu, W.; Yang, C.; Li, D. A gradient theory approach to line tension of liquid-liquid-fluid systems. *Colloids Surf., A* **1998**, *144*, 275−285.
(11) Schimmele, L.; Napiórkowski, M.; Dietrich, S. Conceptual aspects of line tensions. *J. Chem. Phys.* **2007**, *127*, 164715.
(12) Schimmele, L.; Dietrich, S. Line tension and the shape of nanodroplets. *Eur. Phys. J. E* **2009**, *30*, 427−430.
(13) Guzzardi, L.; Rosso, R. Sessile droplets on a curved substrate: effects of line tension. *J. Food Compos. Anal.* **2007**, *40*, 19.
(14) Hienola, A. I.; Winkler, P. M.; Wagner, P. E.; Vehkamäki, H.; Kulmala, M. Estimation of line tension and contact angle from heterogeneous nucleation experimental data. *J. Chem. Phys.* **2007**, *126*, 299.
(15) Checco, A.; Guenoun, P.; Daillant, J. Nonlinear Dependence of the Contact Angle of Nanodroplets on Contact Line Curvature. *Phys. Rev. Lett.* **2003**, *91*, 186101.
(16) Gu, Y.; Li, D.; Cheng, P. Determination of Line Tension from the Shape of Axisymmetric Liquid-Vapor Interfaces around a Conic Cylinder. *J. Colloid Interface Sci.* **1996**, *180*, 212−217.
(17) Gu, Y. Drop size dependence of contact angles of oil drops on a solid surface in water. *Colloids Surf., A* **2001**, *181*, 215−224.
(18) Leelamanie, D. A. L.; Karube, J. Drop size dependence of soil-water contact angle in relation to the droplet geometry and line tension. *Soil Sci. Plant Nutr.* **2012**, *58*, 675−683.
(19) Bauer, C.; Dietrich, S. Quantitative study of laterally inhomogeneous wetting films. *Eur. Phys. J. B* **1999**, *10*, 767−779.
(20) Churaev, N. V.; Starov, V. M.; Derjaguin, B. V. The shape of the transition zone between a thin film and bulk liquid and the line tension. *J. Colloid Interface Sci.* **1982**, *89*, 16−24.
(21) Park, J.-Y.; Ha, M.-Y.; Choi, H.-J.; Hong, S.-D.; Yoon, H.-S. A study on the contact angles of a water droplet on smooth and rough solid surfaces. *J. Mech. Sci. Technol.* **2011**, *25*, 323−332.
(22) Weijs, J. H.; Marchand, A.; Andreotti, B.; Lohse, D.; Snoeijer, J. H. Origin of line tension for a Lennard-Jones nanodroplet. *Phys. Fluids* **2011**, *23*, 021602.
(23) Amp, H. P.; Birkett, G. R. Determination of contact angle by molecular simulation using number and atomic density contours. *Mol. Simul.* **2012**, *38*, 945−952.
(24) Peng, H.; Birkett, G. R.; Nguyen, A. V. The impact of line tension on the contact angle of nanodroplets. *Mol. Simul.* **2014**, *40*, 934−941.
(25) Tolman, R. C.; Richard, C. The Effect of Droplet Size on Surface Tension. *J. Chem. Phys.* **1949**, *17*, 333−337.
(26) Nagayama, G.; Kawagoe, M.; Tokunaga, A.; Tsuruta, T. On the evaporation rate of ultra-thin liquid film at the nanostructured surface: A molecular dynamics study. *Int. J. Therm. Sci.* **2010**, *49*, 59−66.
(27) Zhang, L.; Xu, J.; Chen, Q.; Wang, S. Switchable heat transfer in nano Janus-interface-system. *Int. J. Heat Mass Transfer* **2018**, *127*, 761−771.
(28) Hong, S. D.; Ha, M. Y.; Balachandar, S. Static and dynamic contact angles of water droplet on a solid surface using molecular dynamics simulation. *J. Colloid Interface* **2009**, *339*, 187−195.
(29) Wolansky, G.; Marmur, A. The Actual Contact Angle on a Heterogeneous Rough Surface in Three Dimensions. *Langmuir* **1998**, *14*, 5292−5297.
(30) Wu, D.; Wang, P.; Wu, P.; Yang, Q. Determination of contact angle of droplet on convex and concave spherical surfaces. *Chem. Phys.* **2015**, *457*, 63.
(31) Iwamatsu, M. Four stages of droplet spreading on a spherical substrate and in a spherical cavity: Surface tension versus line tension and viscous dissipation versus frictional dissipation. *Phys. Rev. E* **2018**, *98*, 062801.